Biophysical Journal Volume 75 November 1998 2382–2388

Effect of D57N Mutation on Membrane Activity and Molecular Unfolding of Cobra Cardiotoxin

Chung-Chuan Lo,* Jui-Hung Hsu,# You-Cheng Sheu,§ Chein-Min Chiang,§ Wen-guey Wu,§ Wunshain Fann,*# and Pei-Hsi Tsao#§

*Institute of Atomic and Molecular Sciences, Academia Sinica, Taipei; #Department of Physics and §Laser Medicine Research Center, National Taiwan University, Taipei; and §Department of Life Sciences, National Tsing Hua University, Hsinchu, Taiwan

ABSTRACT Cobra cardiotoxins (CTXs) are able to adopt a three-fingered β-strand structure with continuous hydrophobic patch that is capable of interacting with zwitterionic phospholipid bilayer. In addition to the four disulfide bonds that form the rigid core of CTXs, Asp^{57} near the C-terminus interacts electrostatically with Lys^{2} near the N-terminus (Chiang et al. 1996. *Biochemistry.* 35:9177–9186). We indicate herein, using circular dichroism and the time-resolved polarized tryptophan fluorescence measurement, that Asp^{57} to Asn^{57} (D57N) mutation perturbs the structure of CTX molecules at neutral pH. The structural stability of the D57N mutant was found to be lower, as evidenced by the reduced effective concentration of the 2,2,2-trifluoethanol (TFE)-induced β-sheet to α-helix transition. Interestingly, the single mutation also allows a greater degree of molecular unfolding, because the rotational correlation time of the TFE-induced unfolding intermediate is larger for the D57N mutant. It is suggested that the electrostatic interaction between N- and C-termini also contributes to the formation of the functionally important continuous hydrophobic stretch on the distant end of CTX molecules, because both the binding to anilinonaphthalene fluorescent probe and the interaction with phospholipid bilayer were also reduced for D57N mutant. The result emphasizes the importance of the hydrophobic amino acid residues near the tip of loop 3 as a continuous part of the three-fingered β-strand CTX molecule and indicates how a distant electrostatic interaction might be involved. It is also implicated that electrostatic interaction plays a role in expanding the radius of gyration of the folding/unfolding intermediate of proteins.

INTRODUCTION

Cardiotoxins (CTXs), which constitute a major component of cobra venom, can lyse many cells and cause the membrane depolarization of cardiomyocytes (Dufton and Hider, 1991; Harvey, 1991; Wu, 1997). They adopt a three-fingered β-strand structure, a folding motif that is shared by neurotoxins and muscarinic toxins. In vitro, CTXs were shown to bind to zwitterionic phospholipids via hydrophobic interaction (Chien et al., 1991, 1994; Chiang et al., 1996b) and to anionic glycosaminoglycans (GAGs) via specific electrostatic interactions (Patel et al., 1997; Vyas et al., 1997, 1998; Wu, 1998). Pro^{31}-containing CTXs can penetrate phospholipid membrane, a process believed to play a crucial role in its toxicity, if the hydrophobic thickness of the lipid bilayer matches the length of the continuous hydrophobic stretch of CTXs (Sue et al., 1997; Sun et al., 1997). Interestingly, cell lytic activity of CTXs may also be correlated with its structural stability in the absence of significant conformational change for chemically modified CTXs (Roumestand et al., 1994) or attributed to the differences in the distribution of the positively charged residues in the three-dimensional structures for CTX analogs, which differ only in their N-terminal amino acid (Jang et al., 1997).

The role of acidic amino acid residues in the structural stability of CTXs has been studied by NMR and circular dichroism (CD) spectroscopic techniques (Chiang et al., 1996a). Electrostatic interaction between the N- and C-termini was found to play an important role in the pH-dependent and 2,2,2-trifluoethanol (TFE)-induced conformational change. Specifically, the pK_a of Asp^{59} of CTX A5 from *Naja atra* venom was determined to be lower than 2.3, suggesting that this residue must be locked in electrostatic interaction with the proximal Lys^{2} (Fig. 1). This putative salt bridge must be weaker than the internal salt bridge detected in many proteins, because in CTX A5 the salt bridge is fully exposed to water solvent, as judged in the three-dimensional (3D) structures determined by both NMR and x-ray (Singhal et al., 1993; Sun et al., 1997). Nevertheless, electrostatic interaction in the region should provide additional stabilization to fold the molecule as a three-fingered β-strand structure and thus provide for proper function. Indeed, recent comparison of the hemolytic activity, thermal denaturation, and solution structures of two CTX mutants in the N-terminus (mutation from Leu^{1} to Arg^{1}) fully confirms the prediction (Jang et al., 1997).

The CTXs M1 from *Naja mossambica* and Tγ from *Naja nigricollis* differ by only one residue; Asp^{57} in Tγ is replaced by Asn in CTX M1 and adopts a similar 3D structure (Gilquin et al., 1993). These toxins thus present themselves as a group of readily available, natural mutants in the C-terminus. We therefore perform a series of CD and flu-

Received for publication 1 June 1998 and in final form 24 July 1998.

Address reprint requests to Dr. Wunshain Fann, Institute of Atomic and Molecular Sciences, Academia Sinica, P.O. Box 23-166, Taipei, Taiwan. Tel.: 886-2-236-68237; Fax: 886-2-236-20200; E-mail: fann@gate.sinica.edu.tw.

0006-3495/98/11/2382/07 $2.00

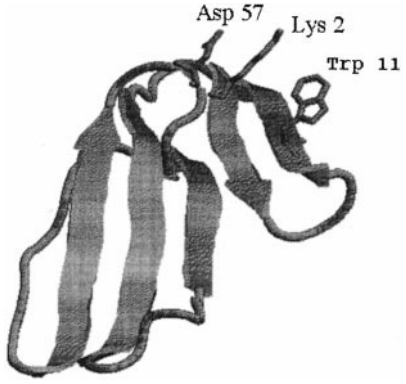

FIGURE 1 Ribbon diagram of Tγ based on its x-ray structure (Bilwes et al., 1994) from *Naja nigricollis*. The proximity of Asp^{57}, Lys^{2}, and Trp^{11} is evident.

orescence spectroscopic investigations on Tγ and its D57N mutant, CTX M1, to compare their structural stability and to understand how the electrostatic interaction near the N- and C-termini could affect the membrane activity of CTXs. (Suffixes A and M denote the origin of snake venom, from *Naja atra* and *Naja mossambica*, respectively.)

MATERIALS AND METHODS

Crude venom from *N. mossambica* and *N. nigricollis* was purchased from Sigma Chemical Company. CTX M1 and CTX Tγ were purified by the procedure of Fryklund and Eaker (1975) and Chien et al. (1994), respectively. Egg sphingomyelin was purchased from Avanti Polar Lipids. Amino acid composition analysis was used to identify the type of CTXs. CTX M1 can be considered to be a mutant of CTX Tγ at position 57 (i.e., Asp^{57} to Asn^{57}), as evidenced by both 2D NMR (O'Connel et al., 1993; Gilquin et al., 1993) and amino acid sequence analysis (Dufton and Hider, 1991; Chien et al., 1994). The purity of CTXs, analyzed by sodium dodecyl sulfate-polyacrylamide gel electrophoresis and analytical reverse-phase high-performance liquid chromatography, was found to be >99%. Protein concentration was determined by the Lowry method.

Aggregation/fusion of sphingomyelin vesicles

Large unilamellar sphingomyelin vesicles were prepared by allowing multilamellar lipid dispersions to extrude through two polycarbonate filters (0.1 μm). The procedure was repeated 10 times, after which gel filtration was performed over Sepharose CL-2B to obtain a homogeneous preparation. The apparent aggregation/fusion activity assay was then performed (Chien et al., 1991, 1994). The turbidity of each sample at 320 nm was determined at 35°C, using a spectrometer, and monitored as a function of time to indicate the aggregation/fusion activity. The maximum and initial turbidity values observed for CTX-induced turbidity change were then defined as 100% and 0% aggregation/fusion activity, respectively. Aliquots of the samples were drawn to examine the origin of the turbidity change, by electron microscopy, in terms of change in vesicle size. The diameters of the freshly prepared vesicles were found to be ~1000 ± 200 Å. The fused vesicle size may enlarge up to μm for samples with maximum turbidity change. Many vesicles appear multilamellar under this condition.

Circular dichroism measurements

TFE-induced structural change was monitored using 20 μM CTX in solutions of different TFE/H_2O ratios. CD spectra were recorded on an AVIV 62A DS spectropolarimeter (Lakewood, NJ) as reported (Chiang et al., 1996a). α-Helix and β-sheet content in CTX for TFE-induced conformational change were quantitated by using CD signals at 222 nm and 195 nm, respectively.

Steady-state anilinonaphthalene binding study

To investigate steady-state anilinonaphthalene (ANS) binding, 100 μM ANS was titrated with CTX Tγ or CTX M1 from 10 μM to 130 μM in 10 mM Tris buffer (pH 7.4). The change of the intensity of ANS fluorescence during titration was measured on a Hitachi F-4010 fluorescence spectrophotometer with an excitation wavelength of 360 nm.

Time-resolved fluorescence measurements

To investigate the fluorescence dynamics of tryptophan during TFE-induced structural transition, time-resolved fluorescence measurements were made by using a time-correlated single photon-counting method. A continuous-wave mode-locked Ti:sapphire laser operated near 870 nm was used, with a 76-MHz repetition rate and a 120-fs pulse width. To excite tryptophan, a homemade third harmonic generator was used to triple the output of the laser to generate a light of 290 nm. A cube polarizer was placed before the sample to ensure that the UV pump light was vertically polarized. The fluorescence was measured perpendicularly to the pump beam. An additional polarizer was placed behind the sample to analyze the fluorescence polarization anisotropy. A monochromator was operated at 348 nm to ensure that only tryptophan fluorescence signals entered the microchannel plate photomultiplier tube detector. The full width at half-maximum (FWHM) response function of the instrument was 100 ps.

The curve fitting of the fluorescence natural and anisotropy decays were performed by the Levenberg-Marquardt least-squares algorithm. In the present experiment, all of the fluorescence decays are best fit using biexponential decay, and all of the fluorescence anisotropy decays roughly follow a single exponential form, that is,

$$r(t) = A_0 e^{-t/\theta_c} \tag{1}$$

where A_o is the initial anisotropy and θ_c is the rotational correlation time. The rotational correlation time for spherical particles is related to the effective hydrodynamic volume of CTXs by the following equation (Steiner, 1991):

$$\theta_c = \frac{\eta V}{kT} \tag{2}$$

where k is Boltzmann's constant, T is the absolute temperature, η is the solvent viscosity, and V is the effective hydrodynamic volume.

Viscosity measurements

To calculate the theoretical value of θ_c of the specific effective hydrodynamic volume, the viscosity of the TFE/H_2O mixture should be determined. The viscosity of the TFE/H_2O mixture was measured with a size 25 Cannon-Ubbelohde viscometer (Cannon Instrument Co.) at ~24°C. The value of the viscosity of each sample was an average of the four repeated measurements.

RESULTS

TFE-induced structural transition as reflected by CD measurement

CTX M1 can be regarded as a natural, single-residue mutant of CTX Tγ; Asp^{57} of Tγ is replaced by Asn^{57} in CTX M1. To define the influence of this mutation on the structure of

CTX, we estimated the structural stability of each toxin by considering its resistance to denaturation as an indication of structural stability. We subjected each toxin to treatment with TFE at different concentrations and studied the change in CTX structure by monitoring the change in ellipticity in the CD spectrum of CTX. Shown in Fig. 2 are the representative CD spectra of CTXs in the presence of TFE (Fig. 2 *A*) and the estimated α-helix content (Fig. 2 *B*) of CTX Tγ and CTX M1, plotted as a function of TFE concentration. In the presence of TFE, all characteristics of the β-sheet spectrum of CTX transformed to all characteristics of α-helix (Fig. 2 *A*). Characteristic CD signals showing α-helical structure with high negative ellipticity at 222 and 208 nm are clearly visible for CTX M1 at TFE concentrations above 80%. For Tγ, on the other hand, ~90% TFE was needed to induce α-helix formation (Fig. 2 *B*). The four disulfide bonds remained intact during this β-sheet to α-helix transition. Hence it is proved that the TFE-induced structural transition is governed by the stability of the CTX, rather than by the intrinsic α-helix formation propensity (Chiang et al., 1996a). Therefore, we conclude that D57N mutation reduces the structural stability of CTX with β-strand structure.

Fluorescence natural decay under the influence of TFE

Fig. 3 *A* shows representative decay in intrinsic fluorescence of CTX Tγ at 25°C, pH 6.0, at the indicated TFE concentration. More than one relaxation process is needed to explain the nonlinearity of the semilog plot of natural fluorescence decay. The result obtained in water (0% TFE) resembles that of Blandin et al. (1994). Their data, which

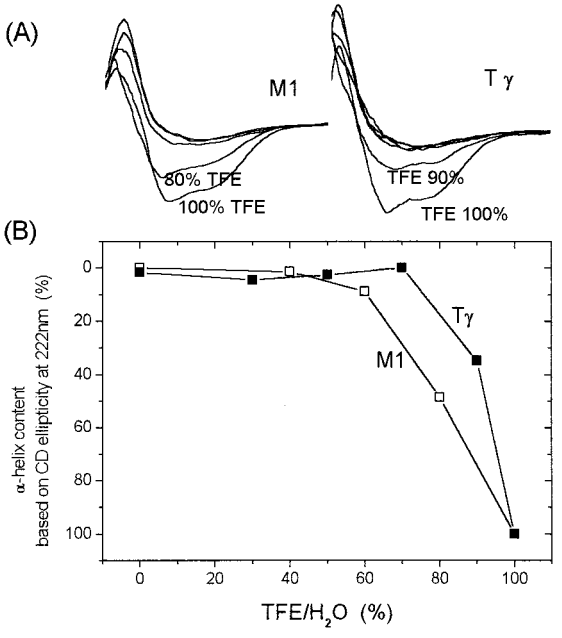

FIGURE 2 (*A*) TFE induces α-helix formation in the β-sheet CTX Tγ and CTX M1, as evidenced by their CD spectra. (*B*) The determined α-helix content based on CD ellipticity at 222 nm.

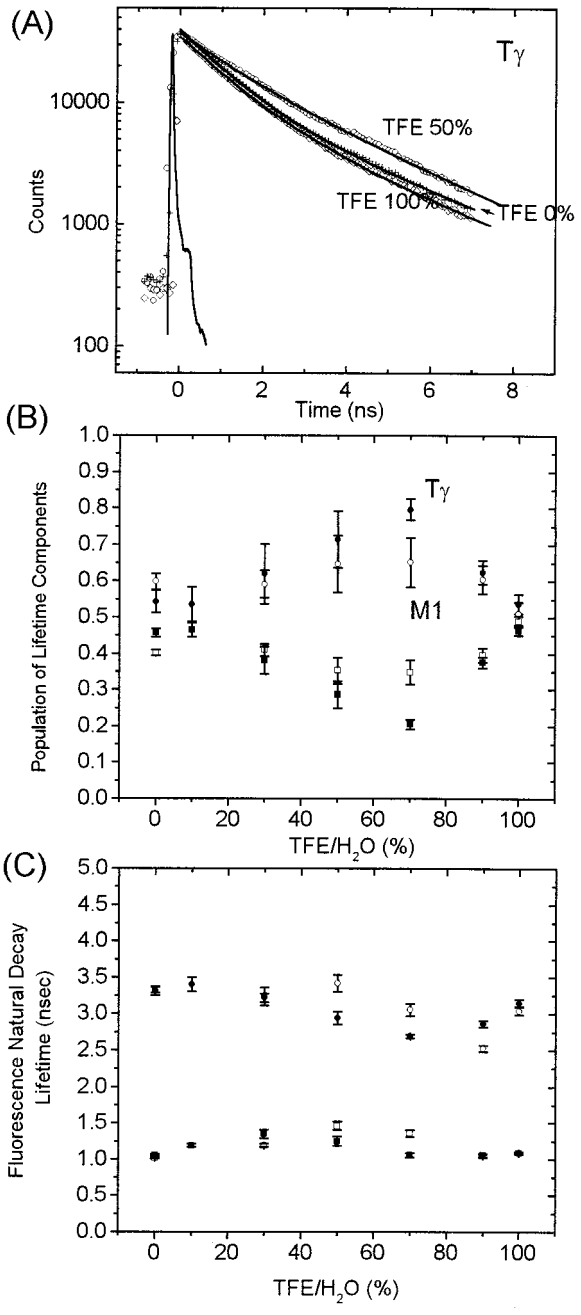

FIGURE 3 (*A*) Fluorescence decay profiles of CTX Tγ at the designated TFE concentration. (*B*) The fluorescence lifetime and (*C*) amplitude of fluorescence lifetime after two exponential decay analyses. The error bars indicate the standard errors from the nonlinear least-squares fitting.

were fitted by the maximum entropy method, showed a wide distribution of lifetime, with two major components centered at 2.05 (68%) and 0.71 (28%) ns. Using two exponential decay terms, we obtained two relaxation times, ~3.3 and 1.0 ns, with respective populations of 45% and 55%. Our results are consistent with those of Blandin et al. (1994).

The distribution of fluorescence natural decay lifetimes, analyzed by using a combination of two exponential decays,

is shown in Fig. 3, *B* and *C*. Both toxins exhibit fluorescence natural decay through two-step processes with comparable lifetimes of ~3 and 1 ns (Fig. 3 *C*). However, the respective populations under the influence of TFE are significantly different (Fig. 3 *B*). Within experimental error and with the exception of decay in the presence of 100% TFE, the population of the two fluorescence decay components of CTX M1 remains constant. On the other hand, the population of the fluorescence natural decay component with a lifetime of 3.3 ns increases from 55% to 80% for CTX Tγ (Fig. 3 *B*), whereas the population for the same fluorescence decay component remains at 60% for CTX M1. This difference implies that the acidic Asp^{57} modulates the fluorescence of Trp^{11} in the presence of TFE. Because Asp^{57} is distant from Trp^{11} (Fig. 1), this acidic residue is unlikely to directly modulate the fluorescence of the fluorophoric Trp^{11}. It is therefore conceivable that TFE attenuates the electrostatic attraction between Asp^{57} and Lys^{2}.

Our result suggests that Lys^{2} modulates the distribution of fluorescence lifetimes. A similar suggestion, although based only on the structural model, was made by Blandin et al. The effect, however, is a change in relative distribution of Trp^{11} fluorescence decay, rather than a change in lifetimes. In aqueous solution, the fluorescence lifetimes of the two toxins are indistinguishable. Asp^{57} can thus be concluded to principally modulate the relative population of the two existing fluorescence lifetime components.

Fluorescence anisotropy decay under the influence of TFE

Blandin et al. demonstrated that the decay in fluorescence anisotropy of Trp^{11} of CTX Tγ can be represented by a single exponential term and that the decay reflects the size and shape of a fairly rigid protein. A plot of the apparent rotational correlation time, θ_c, versus η/T is linear, although a slight upward curvature is evident. The linearity suggests that the Einstein-Stokes relation can be applied to the CTX molecule in water, at least to a first-order approximation.

Shown in Fig. 4 are the apparent rotational correlation times determined by fluorescence anisotropy decay, with the single-exponential term of Trp^{11} for CTX M1 and CTX Tγ as a function of TFE concentration. A theoretical line calculated using Eq. 2 is also plotted for comparison. We assumed that the Stokes radii are ~15 Å, a value comparable to the dimension of the CTX Tγ, estimated from NMR and x-ray data. The viscosity of the TFE/H_2O mixture, as shown in Table 1, was determined using a viscometer as described in Viscosity Measurements, above. For CTX Tγ, all of the values of the measured rotational correlation time fall on the theoretical line. The good fit suggests that the molecular dimension of CTX Tγ remains unchanged during the experiment. However, for CTX M1, the measured rotational correlation time is significantly higher than the theoretical value estimated for TFE concentration, from 30% to 70%, just before the transition to α-helix occurs. The higher

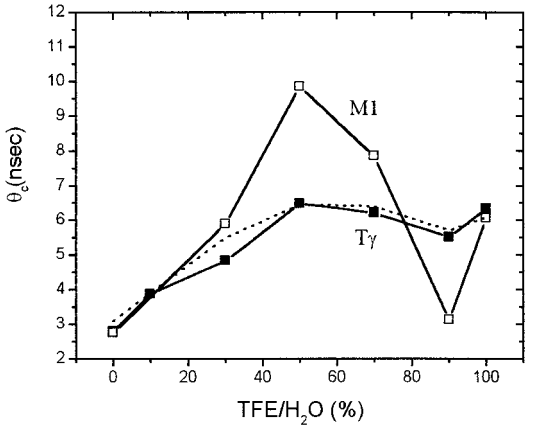

FIGURE 4 Apparent rotational correlation time, θ_c, of CTX M1 and CTX Tγ plotted against concentration of TFE. Dashed lines represent the estimated theoretical curve, using a Stokes's radius of 15 Å and the measured viscosity.

correlation time of CTX M1 is not due to the TFE-induced aggregation of CTX molecules, because it is independent of the concentration of CTX M1 from 2.0 to 40 μM (data not shown). One of the simplest explanations is that the molecular dimension of the CTX M1 molecule expands under this experimental condition.

We have shown, thus far, that by using CD and time-resolved fluorescence polarization measurements, CTX M1 and Tγ display delicate differences. First, the D57N mutation perturbs the structural stability of CTX Tγ, because the amount of TFE needed to induce β-sheet to α-helix transition is lower. Second, in the absence of the putative Asp^{57} to Lys^{2} interaction, the molecular dimension of CTX M1 expands between TFE concentrations of 30% and 70%, as reflected by the increased rotational correlation time, θ_c. Expansion occurs via an unfolded intermediate in the TFE-induced β-sheet to α-helix transition. The latter observation suggests that reduced electrostatic interaction increases the radius of gyration, as observed in the folding intermediate of CTX M1. Similar phenomena are also observed for other proteins (Elizer et al., 1995; Tan et al., 1996).

Fig. 5 shows a schematic model to explain the difference between TFE-induced unfolding of CTX M1 and Tγ, as consistent with CD and fluorescence measurements. Despite the similarity in their overall 3D structure, the unfolding intermediate in TFE-induced structural transition appears to be significantly different, depending on the presence of putative electrostatic interaction between Asp^{57} and Lys^{2}. This is an interesting observation in comparison with other α-helix proteins, apomyoglobin or cytochrome *c*

TABLE 1 The viscosity of TFE/H_2O mixtures at 24°C

Volume ratio	0/100	10/90	30/70	50/50	70/30	90/10	100/0
Viscosity (mPa S)	0.92	1.16	1.63	1.91	1.90	1.69	1.81

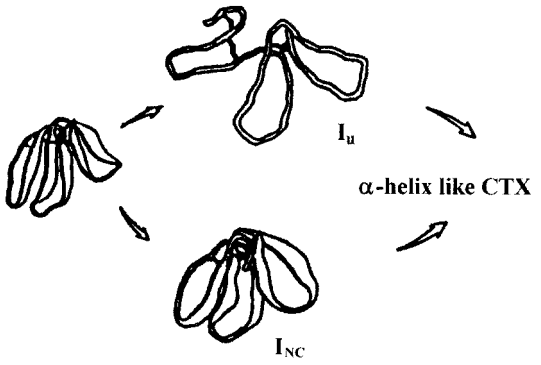

FIGURE 5 A hypothetical model to explain the mechanism of TFE-induced unfolding of CTX Tγ and CTX M1. The N57D mutation in CTX M1 reduces electrostatic interaction between C- and N-termini in I_{NC} intermediate of CTX Tγ and causes expansion of molecular dimension of I_U intermediate, as reflected by the higher fluorescence anisotropy decay time shown in Fig. 4.

(Kay and Baldwin, 1996; Marmorino and Pielak, 1995), in which protein-specific hydrophobic interaction between N- and C-terminal helices guides the formation of the folding intermediate, I_{NC}, of cytochrome *c* (Colon et al., 1996). Furthermore, disruption of this hydrophobic interaction destabilizes the molten globule state to the same extent that it destabilizes the native state (Ptitsyn, 1996).

CTX-induced aggregation/fusion of sphingomyelin vesicles

Only the structural differences between the two toxins appear to have been demonstrated thus far for denaturation, and the importance of this study to the biological function of CTX can be questioned. We therefore searched for differences between two CTXs in a functional context. We have shown earlier that CTX can induce aggregation/fusion of phospholipid vesicles around the lipid phase transition temperature (Chien et al., 1991). This ability of CTX is derived from the solubilization action of its continuous hydrophobic region, formed by the tips of three-finger loops (Sun et al., 1997; Sue et al., 1997). TFE is often used as an artificial mimic of the lipid environment, because of its low dielectric constant, to study membrane proteins. For these reasons, we studied the effect of D57N mutation on the membrane-related activity of CTXs.

Shown in Fig. 6 *A* are the dose dependence curves of CTX-induced aggregation/fusion activity of sphingomyelin vesicles, as monitored by their turbidity measurement at 320 nm. The dose-response curve for the action of CTX Tγ can be described by the Hill equation and a single K_d value, whereas for CTX M1 it is more complicated. Nevertheless, the potencies of the two studied CTXs are clearly different. Furthermore, the relative potencies of the two toxins correlate with their structural stabilities. About 25 μM CTX Tγ, but 35 μM CTX M1, is needed to produce 50% aggregation/fusion activity. Therefore, the membrane-related activity of

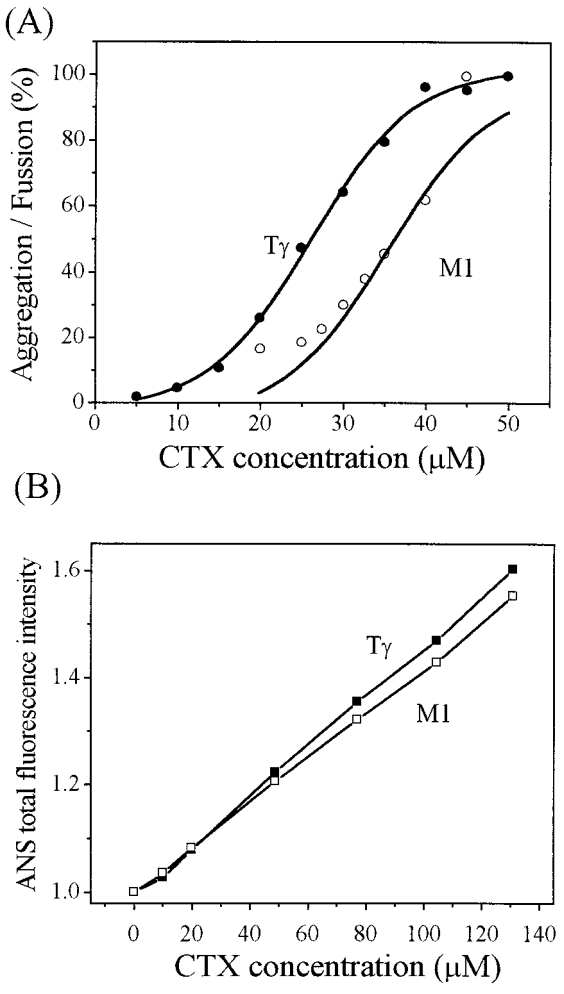

FIGURE 6 The effect of D57N mutation on the membrane-related activity of CTX as monitored by (*A*) the CTX-induced aggregation/fusion of sphingomyelin vesicles and (*B*) ANS binding activity. The total fluorescence is the integral of measured fluorescence intensity over the wavelength from 400 nm to 600 nm.

CTX M1 is ~50% weaker than that of CTX Tγ. This difference in activity can only be attributed to D57N mutation.

To understand whether D57N mutation also produces changes in the hydrophobic domain, which is presumably responsible for the CTX-induced aggregation/fusion activity of sphyingomyelin vesicles, we also performed an ANS binding study (Fig. 6 *B*). Our results indicate that D57N can result in a delicate change in the hydrophobic domain and impair the hydrophobic interaction of CTX M1 with phospholipid bilayers.

DISCUSSION

CTX M1 and Tγ, differing by one amino acid at position 57, are natural mutants. High-resolution 2D NMR spectroscopy revealed that the 3D solution structures of the two molecules are superimposable (Gilquin et al., 1993; O'Connel et al., 1993). Not only are the distance and the dihedral angle constraints of the two molecules similar, but the overall

chemical shifts of the main chain protons are identical. Interestingly, ~25% of CTXs with known amino acid sequences incorporate different residues at position 57. Therefore, it is interesting to learn if the D57N mutation in CTXs plays a structural and/or functional role.

We showed in this study that the mutation might impair the electrostatic interaction of the CTX molecule between the N- and C-termini and thereby decrease the structural stability of CTX M1. Weakened association between the N- and C-termini causes the molecular dimensions of CTX to expand during unfolding. More importantly, the hydrophobic domain and thus the membrane-related activity of CTXs are perturbed as a result of facile unfolding of CTX M1: CTX-induced aggregation/fusion of phospholipid vesicles is significantly reduced. Because CTX M1 is more amenable to unfolding, the compactness of the CTX structure is lost, and the steric arrangement of the cationic cluster and of the continuous hydrophobic stretch is disturbed. This disruption in the structure possibly weakens the binding of the toxin to phospholipid membrane in penetration form. Specifically, the detachment of hydrophobic residues Leu^{45}, Leu^{46}, and Val^{47} of loop 3 and the cationic Lys^{50} from the neighboring loop 2 prevent effective association of CTX with phospholipid membranes. This observation emphasizes the role of hydrophobic amino acid residues of loop 3 as important mediators in forming the continuous structural domain for the effective functioning of loops 2 and 1.

The structural stability of CTX Tγ dictates its cytolytic activity; the dynamic perturbation of the phospholipid binding site in chemically modified Tγ causes a decrease in toxicity of the derivatives (Roumestand et al., 1994). A similar conclusion was also made for CTX A5 based on the pH-dependent membrane binding behavior of the toxin (Chiang et al., 1996b). This observation suggests that the structural stability of CTX A5 is "perturbed" at neutral to acidic pH. We have shown here that the structural stability also plays a role in the interaction of CTX with phospholipid membranes. It is concluded that the stability of CTX molecules, in addition to its three-dimensional structure, also plays a role in its biological activity.

Our results can also be used to explain the following two recent observations. First, Blandin et al. showed that Trp^{11} of CTX Tγ exhibits a broad and complex distribution of fluorescence lifetimes. They suggested that Lys^2 and Lys^{60} play a role because of their proximity to Trp^{11}, as evident in the 3D structure of CTX Tγ (Bilwes et al., 1994; Fig. 1). We showed in this study that CTX M1 also exhibits a broad distribution in fluorescence lifetimes, but the relative population of fluorescence lifetimes, as affected by TFE, is significantly different from those of Tγ. Trp^{11} lies at the antiparallel β-strand in the loop 1 region, proximal to Lys^2; the latter residue lies in the same loop (Fig. 1). The flexible Lys^2 and/or Lys^{59} (near the C-terminal) may modulate the fluorescence lifetime of Trp^{11}. Our results suggest that the distribution of lifetimes can also be modulated by the distant Asp^{57}. Because Asn^{57} appears to exert a small effect on the studied lifetime distribution, the effect can best be attributed to electrostatic interaction between Asp^{57} and Lys^2. Characterization of the two fluorescence lifetimes may aid future study of the dynamics of Trp^{11}-containing CTXs.

Second, TFE and guanidinium chloride (GdmHCl) induce α-helical and random coil conformation, respectively, in nine CTXs. The structural stability of β-sheet, rather than a propensity for α-helix formation, dictates the TFE-induced structural transition of CTXs (Chiang et al., 1996a). It was suggested that disruption of electrostatic interaction between N- and C-termini generates an unfolded intermediate, which transforms to α-helix. The idea is indeed supported by the expanded molecular dimension of CTX M1, as indicated by the study of time-resolved fluorescence anisotropy decay. Therefore, the electrostatic interaction plays a role in expanding the radius of gyration of the unfolding intermediate of proteins. This suggestion is in contrast to that of other α-helix proteins of cytochrome *c*, where the hydrophobic interaction plays a dominant role (Kay and Baldwin, 1996; Marmorino and Pielak, 1995).

C. C. Lo and W. Fann acknowledge Prof. Robert Austin for his stimulating discussions. We also thank Ms. Yi-Shiuan Liu for her sample preparations and Mr. Kuo-Kan Liang for his discussions on data fitting.

This work was supported by the National Science Council, Taiwan (grants 85-2113-M007-035Y, 85-2311-B-002-050, and 87-2112-M001-045).

REFERENCES

Blandin, P., F. Merola, J. Brochon, O. Tremeau, and A. Menez. 1994. Dynamics of the active loop of snake toxins as probed by time-resolved polarized tryptophan fluorescence. *Biochemistry.* 33:2610–2619.

Chiang, C.-M., S.-L. Chang, H.-J. Lin, and W. Wu. 1996a. The role of acidic amino acid residues in the structural stability of snake cardiotoxins. *Biochemistry.* 35:9177–9186.

Chiang, C-M., K-Y. Chien, H-J. Lin, J-F. Lin, H-C. Yeh, P-I. Ho, and W. Wu. 1996b. Conformational change and inactivation of membrane phospholipid-related activity of cardiotoxin V from Taiwan cobra venom at acidic pH. *Biochemistry.* 35:9167–9176.

Chien, K-Y., C.-M. Chiang, Y.-C. Hseu, A. A. Vyas, G. S. Rule, and W. Wu. 1994. Two distinct types of cardiotoxin as revealed by the structure and activity relationship of their interaction with zwitterionic phospholipid dispersions. *J. Biol. Chem.* 269:14473–14483.

Chien, K-Y., W-N. Huang, J-H. Jean, and W. Wu. 1991. Fusion of sphingomyelin vesicles induced by proteins from Taiwan cobra (*Naja naja atra*) venom. *J. Biol. Chem.* 266:3252–3259.

Colon, W., G. A. Elove, P. Wakem, F. Sherman, and H. Roder. 1996. Side chain packing of the N- and C-terminal helices plays a critical role in the kinetics of cytochrome *c* folding. *Biochemistry.* 35:5538–5549.

Dufton, M.-J., and R. C. Hider. 1991. The structure and pharmacology of elapid cytotoxins. *In* Snake Toxins. A. L. Harvey, editor. Pergamon Press, New York. 259–302.

Eliezer, D., P. A. Jennings, P. E. Wright, S. Doniach, K. O. Hodgson, and H. Tsuruta. 1995. The radius of gyration of an apomyoglobin folding intermediate. *Science.* 270:487–488.

Gilquin, B., C. Roumestand, S. Zinn-Justin, A. Menez, and F. Toma. 1993. Refined three-dimensional solution structure of a snake cardiotoxin: analysis of the side-chain organization suggests the existence of a possible phospholipid binding site. *Biopolymer.* 33:1659–1675.

Harvey, A. L. 1991. Reptile venoms and toxins. *In* Reptile Venoms and Toxins. A. T. Tu, editor. Marcel Dekker, New York. 85–106.

Jang, J.-Y., T. K. S. Kumar, G. Jayaraman, P.-W. Yang, and C. Yu. 1997. Comparison of the hemolytic activity and solution structures of two snake venom cardiotoxin analogues which only differ in their N-terminal amino acid. *Biochemistry.* 36:14635–14641.

Kay, M. S., and R. L. Baldwin. 1996. Packing interactions in the apomyglobin folding intermediate. *Nature Struct. Biol.* 3:439–445.

Marmorino, J. L., and C. L. Pielak. 1995. A native tertiary interaction stabilizes the A state of cytochrome *c*. *Biochemistry.* 34:3140–3143.

O'Connel, J. F., P. E. Bougis, and K. Wuthrich. 1993. Determination of the nuclear magnetic resonance solution structure of cardiotoxin CTX IIb from *Naja mossambica mossambica*. *Eur. J. Biochem.* 213:891–900.

Patel, H. V., A. A. Vyas, K. A. Vyas, C.-M. Chiang, L.-M. Chi, and W. Wu. 1997. Heparin and heparan sulfate bind to snake cardiotoxin. *J. Biol. Chem.* 272:1484–1493.

Ptitsyn, O. 1996. How molten is the molten globule. *Nature Struct. Biol.* 3:488–490.

Roumestand, C., B. Gilquin, O. Tremeau, E. Gatineau, A. Mouawad, A. Menez, and F. Toma. 1994. Proton NMR studies of the structural and dynamical effect of chemical modification of a single aromatic sidechain in a snake cardiotoxin. Relation to the structure of the putative binding site and the cytolytic activity of the toxin. *J. Mol. Biol.* 243: 719–735.

Singhal, A. K., K-Y. Chien, W. Wu, and R. S. Rule. 1993. Solution structure of cardiotoxin V from *Naja naja atra*. *Biochemistry.* 32: 8036–8044.

Steiner, R. F. 1991. Fluorescence anisotropy: theory and applications. *In* Topics in Fluorescence Spectroscopy, Vol. 2. J. R. Lakowicz, editor. Plenum Press, New York. 1–52.

Sue, S-C., P. K. Rajan, T.-S. Chen, C.-H. Hsieh, and W. Wu. 1997. Action of Taiwan cobra cardiotoxin on membranes: binding modes of a β-sheet polypeptide with phosphatidylcholine bilayers. *Biochemistry.* 36: 9826–9836.

Sun, Y-J., W. Wu, C-M. Chiang, A-Y. Hsin, and C-D Hsiao. 1997. Crystal structure of cardiotoxin V from Taiwan cobra venom: pH-dependent conformational change and a novel membrane-binding motif identified in the three-finger loops of P-type cardiotoxin. *Biochemistry.* 36: 2403–2413.

Tan, Y-J., M. Oliverberg, and A. R. Fersht. 1996. Titration properties and thermodynamics of the transition state for folding: comparison of two-state and multi-state folding pathways. *J. Mol. Biol.* 264:377–389.

Vyas, A. A., J.-J. Pan, H. V. Patel, K. A. Vyas, C.-M. Chiang, Y.-C. Sheu, J.-K. Hwang, and W. Wu. 1997. Analysis of binding of cobra cardiotoxins to heparin reveals a new β-sheet heparin-binding structural motif. *J. Biol. Chem.* 272:9661–9670.

Vyas, K. A., H. V. Patel, A. A. Vyas, and W. Wu. 1998. Glycosaminoglycans bind to homologous cardiotoxins with different specificity. *Biochemistry.* 37:4527–4534.

Wu, W. 1997. Diversity of cobra cardiotoxin. *J. Toxicol. Toxin Rev.* 16:115–134.

Wu, W. 1998. Cobra cardiotoxin and phospholipase A2 as GAG binding toxins: on the path from structure to cardiotoxicity and inflammation. *Trends Cardiovasc. Med.* (in press).